J. Fluid Mech. (2003), *vol.* 480, *pp.* 1–24.
DOI: 10.1017/S0022112002003154 Printed in the United Kingdom

An experimental investigation of the direct initiation of cylindrical detonations

By M. I. RADULESCU[1], A. J. HIGGINS[1], S. B. MURRAY[2] AND J. H. S. LEE[1]

[1]Department of Mechanical Engineering, McGill University, Montreal, Canada H3A 2K6

[2]Defence Research Establishment Suffield, Ralston, Canada T0J 2N0

(Received 4 May 2001 and in revised form 5 September 2002)

The direct initiation of gaseous detonation is investigated experimentally in the cylindrical geometry. By using a long source of energy deposition along a line (i.e. pentaerythritoltetranitrate (PETN) detonating cord), undesirable charge initiation and confinement effects are eliminated. This permitted the different flow fields of direct initiation of detonation to be studied unambiguously. Although the detonation velocity in the detonating cord is finite, it was sufficiently large compared to the acoustic velocity in the surrounding gas to permit the different flow fields to be investigated within the hypersonic analogy framework, by which the detonating cord synchronizes a continuous series of cylindrical initiation events along its length. The hypersonic approximation was validated in experiments conducted in a non-reactive medium (air). In the supercritical regime of initiation in combustible gas, stable oblique detonations were observed, confirming their existence and stability. In the critical regime, the onset of detonation was observed to occur consistently from stochastic detonative centres. These centres appeared during the initial decay of the blast wave to sub-Chapman–Jouguet (CJ) velocities. The photographic evidence revealed the three-dimensional details of the detonation kernels' amplification. The present results in the cylindrical geometry are further used to discuss criteria for direct initiation of detonations. In conjunction with previous experiments in the spherical and planar geometries, a criterion for direct initiation is found to involve a critical decay rate of the reacting blast wave. In light of the experimental evidence of the inherent three-dimensional effects during the initiation phase, the strict one-dimensionality of current theoretical models is discussed.

1. Introduction

Direct initiation of detonation refers to the 'instantaneous' initiation of a self-propagating detonation wave by a strong blast wave. Experimental evidence suggests that for a given unconfined combustible mixture, successful initiation of a detonation wave depends solely on the amount of energy deposited at the source, provided the energy is deposited sufficiently fast (Lee 1977). For this reason, such experiments provide a simple and accurate measure for the sensitivity and explosion hazards of different gaseous combustible mixtures. Theoretically, the problem has attracted much attention owing to the simplicity of the initial conditions: a decaying self-similar blast wave triggers chemical reactions in its wake by adiabatic shock compression. For a sufficiently slow characteristic time of decay of the blast, equivalent to a high-energy source, the chemical reactions remain coupled to the leading shock front and form

a self-sustained detonation wave. Alternatively, for a fast decay of the blast wave, the chemical reactions decouple from the blast front. Since the pioneering work of Zeldovich, Kogarko & Simonov (1956), numerous theoretical models based on a one-dimensional assumption have been formulated (e.g. He & Clavin 1994; Eckett, Quirk & Shepherd 2000), and their predictions compared with experimentally measured critical source energies. A review of these models can be found in Lee & Higgins (1999). However, such theoretical efforts have not yielded a consensus among the different investigations, largely because of the inability to resolve experimentally the flow fields close to the energy source, where the onset of detonation occurs.

The point source of energy required for the direct initiation of spherical detonations appears to be the easiest geometry to realize experimentally. Benedick *et al.* (1986), for example, present experimental measurements of the critical mass of condensed explosive required to initiate spherical detonations in various hydrocarbon–air mixtures. Owing to the rapid release of the large energy density in high explosives, this technique appears to be the most suitable to simulate the point-source self-similar blast motion for intense explosions and estimate the amount of energy deposition. For these reasons, this technique is readily amenable to theoretical modelling. However, severe non-idealities are present in attempting to initiate detonations via spherical high-explosive charges. Difficulties in uniformly initiating the high-explosive charge itself led to inherent non-symmetrical detonations in the initiator charge and non-uniform burning. As a result, large parts of the unreacted explosive serve as projectiles and interact with the gaseous flow field of interest. These complications may promote the onset of detonation in the gas (Komatsu & Takayama 2000). For this reason, such studies can only yield approximate values of critical energies and provide limited insight into the gasdynamic phenomena and local flow fields present prior and during the onset of detonation.

Of equal theoretical and practical interest is the initiation of planar and cylindrical detonations. However, their experimental implementation, which requires, respectively, instantaneous planar and line sources of energy, presents considerable challenges. Prior experiments with the initiation of cylindrical detonations have used either spark gaps (Matsui & Lee 1976) or exploding wires (Vasil'ev 1983; Aminallah, Brossard & Vasil'ev 1993), where the amount of energy deposited is difficult to estimate. Furthermore, the lengths of the line sources as well as the amounts of energy that can be deposited are limited. The limited length of the spark gap or exploding wire necessitates the use of a narrow chamber, and hence introduces significant interaction with the chamber walls. Non-idealities due to confinement effects are also present in investigations using condensed explosive charges to initiate cylindrical detonations in a narrow chamber (Vasil'ev & Grigoriev 1980).

Higgins, Radulescu & Lee (1998) have shown that the direct initiation of cylindrical detonations can be studied by using a long line charge of high explosive (detonating cord) as the energy source. Since the cord does not liberate its energy instantaneously, but at the rate of the detonation velocity in the high explosive of the cord (≈ 6–$7\,\mathrm{km\,s^{-1}}$), this technique provides a time sequence of cylindrical initiation events synchronized by the detonation velocity in the cord. Since the detonation velocity in the cord is more than an order of magnitude greater than the characteristic sound velocity in the surrounding gas (i.e. a Mach number of approximately 20), the flow field becomes decoupled in the axial direction and is referred to as quasi-cylindrical. The flow field from a detonating cord can be treated under the hypersonic similarity assumption (Chernyi 1961), and can thus be viewed as a series of cylindrical initiations, synchronized by the rate of energy release along the cord's length. In this sense, the

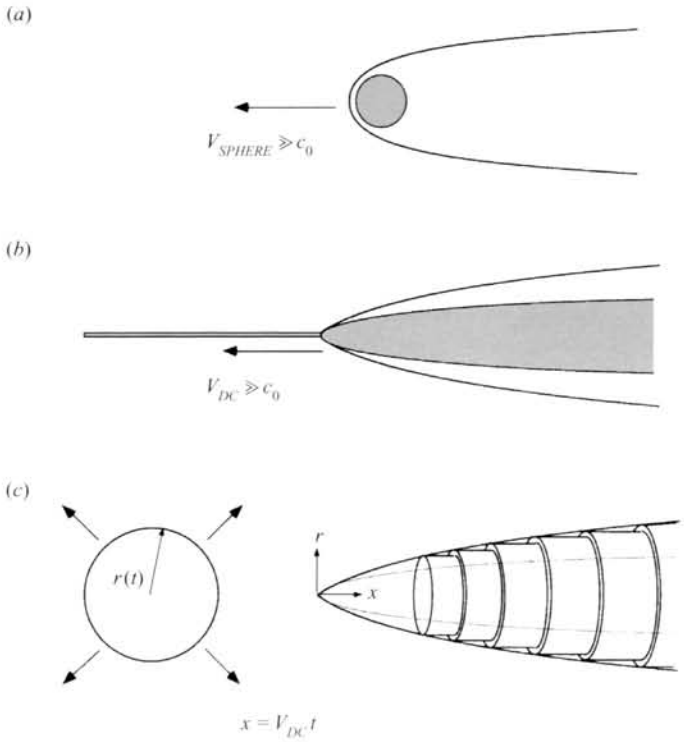

FIGURE 1. The hypersonic cylindrical blast wave analogy: (*a*) the bow shock around a hypersonic sphere, (*b*) the bow shock around a high explosive detonating cord, and (*c*) the blast wave analogy illustrating the sequence of cylindrical blast waves synchronized by the velocity in the detonating cord V_{DC}.

results obtained along a sufficiently long cord represent statistically representative samples of multiple initiation events. A sketch of the resulting flow field is shown in figure 1. Furthermore, since the detonating cord can be made arbitrarily long, such a technique permits eliminating any detrimental end effects (e.g. confinement, charge initiation), and thus provides a clean initiation source to unambiguously study the flow fields in direct initiation. However, the use of a small detonation chamber in the study of Higgins *et al.* (1998) limited their investigation to a narrow range of mixture compositions and did not permit flow visualization of the different flow fields.

The study of direct initiation from a rapidly moving energy source, such as the detonating cord, is also intimately linked with the problem of detonation initiation by a hypersonic projectile travelling through a gaseous detonable mixture. The parallel between the detonating cord and the high-velocity projectile problems is shown in figure 1, where both the projectile and the expanding high-explosive products deposit their energy by doing work on the surrounding gas and drive similar conical blast waves. Of particular interest are the critical conditions necessary for the establishment of a conical detonation wave in the surrounding combustible gas. Under the hypersonic blast-wave analogy, Lee (1997) and Vasil'ev (1994) relate the energy deposited by the moving projectile to the energy from an equivalent line-source of energy. In this sense, the ability to predict the critical energy for the direct initiation of a cylindrical detonation provides a first-order estimate on the critical conditions for detonation initiation by a hypervelocity projectile. Furthermore, the stability of

the resulting oblique detonation initiated around a projectile is of significance to applications that seek to stabilize oblique detonation waves in propulsion applications (Pratt, Humphrey & Glenn 1991; Shepherd 1994). To date, the limited velocities of gas-gun-launched projectiles, which are of the order of the Chapman–Jouguet (CJ) detonation velocity ($\approx 2\,\mathrm{km\,s^{-1}}$), has not permitted observation of steady oblique detonation waves. The existence and stability of oblique detonation waves remain to be confirmed.

The prime objective of the present paper is thus to clarify the different flow fields which arise through the direct initiation of cylindrical detonations. Through the photographic observation of the details of the different flow fields and the critical conditions for direct initiation, different theoretical models and the assumptions therein can be validated. The high-explosive detonating cord technique of Higgins *et al.* (1998) is adopted in order to obtain a clean energy source and to permit the direct initiation of cylindrical detonations to be observed over a wide range of mixture sensitivity and source energies. Direct flow visualization is employed to study the different flow fields. The present paper is comprised of five sections. Section 2 presents a brief description of the experimental details. In § 3, the initiating blast waves from detonating cords are first analysed in a non-reactive medium (air) in order to verify the hypersonic similarity assumption and determine its domain of validity. Section 4 presents the experimental results obtained in combustible gas for direct initiation of detonations. Subsequent discussion on the pertinence of the present results and comparison with recent models for direct initiation of detonation follow in § 5.

2. Experimental details

The large-scale experiments were performed at the Defence Research Establishment Suffield (DRES), Alberta, Canada. Large 8 m long and 2 m diameter thin-walled plastic bags filled with the desired fuel–air mixtures were used. The experimental set-up is shown in figure 2. The different pentaerythritoltetranitrate (PETN) detonating cords used as energy source in this study and their respective energy contents are given in table 1. The amount of energy deposition by the cord is estimated from the heat of detonation of PETN ($Q_{PETN} = 6.332\,\mathrm{kJ\,g^{-1}}$, taken from Dobratz & Crawford 1985). The detonating cord was positioned axially inside the bag, running along the entire length of the bag. To prevent sagging due to gravity, one end of the detonating cord was attached to an elastic band under tension. The detonating cord was initiated at the other end by a Reynolds detonator placed outside the bag. The first 0.9 m of the detonating cord was confined by a strong steel casing to prevent any interaction between the blast wave from the cord and the support structure when the detonation in the cord enters the bag.

The experiments were conducted at ambient atmospheric conditions ($P_0 = 0.92$ bar, $T_0 = 15 \pm 5\,^{\circ}\mathrm{C}$). Ethylene ($C_2H_4$) was used as the fuel for all the tests. Air at atmospheric conditions was used as the oxidizer. The mixtures were prepared by continuous fuel injection and mixture recirculation inside the bag, until the desired concentration was reached. The composition of the mixture was monitored by an infrared mass spectrometer (Wilks Miran 80) via continuous sampling. This system guaranteed the mixture concentration to within $\pm 0.05\%$ ethylene in air. After a uniform mixture was obtained, the recirculation fan was stopped before firing.

Each experiment was monitored by ionization probes, pressure transducers and high-speed cameras. Ionization probes placed directly on the cord measured the

PETN content ($g\,m^{-1}$)	Equivalent line energy E_S ($kJ\,m^{-1}$)	Cylindrical explosion length $R_0 = (E_S/P_0)^{0.5}$ (m)
4.9	31	0.58
10.6	67	0.85
14.8	94	1.01
21.2	134	1.21
42.4	269	1.71
84.8	537	2.42

TABLE 1. PETN detonating cords used in this study, their energy content and the corresponding explosion length.

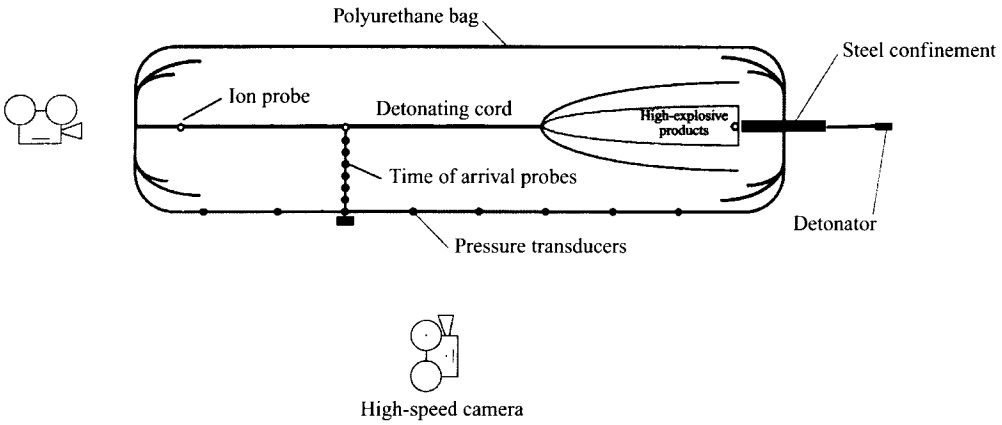

FIGURE 2. The experimental set-up.

time of arrival of the detonation in the PETN at the fixed probe location. These measurements also provided a timing reference with the events in the surrounding combustible gas. Piezoelectric pressure transducers mounted 1 m apart along the bag boundary measured the strength and time-of-arrival of the generated blast wave (or detonation). For certain tests, a radial probe of contact gauges was positioned perpendicular to the detonating cord inside the plastic bag. These pressure-sensitive contact probes consisted of 0.025 mm thick brass disks, 4 mm in diameter, separated by a thin 0.05 mm gap, which recorded the time of arrival of the shock wave or detonation. The different times of arrival along the cord, perpendicular to the cord, and at the pressure transducers at the bag boundary permitted measurement of: (i) the detonation velocity in the PETN cord, (ii) the shock radial trajectory and velocity, and (iii) the velocity of the shock as it sweeps along the bag.

Self-luminous high-speed video and cinematography with side-on and end-on views were used for the visualization of the entire flow field. The high-speed cinematography and digital video, with maximum framing rates of 7000 frames s^{-1} and 1000 frames s^{-1}, respectively, captured the self-luminous combustion front in the gaseous mixture and the detonating cord products. This technique did not permit direct observation of the shock wave in the gaseous mixture. Observation of the shock would require shadowgraph/schlieren photography, which are extremely difficult to implement in large-scale field trials.

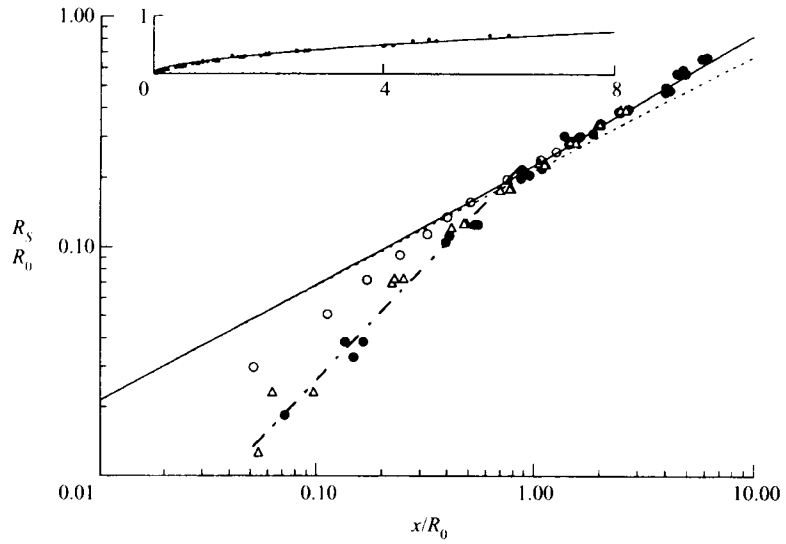

FIGURE 3. Normalized blast wave trajectories in air from long PETN detonating cords: ○, $E_S = 537\,\mathrm{kJ\,m^{-1}}$; △, $E_S = 94\,\mathrm{kJ\,m^{-1}}$; ●, $E_S = 31\,\mathrm{kJ\,m^{-1}}$; ..., self-similar solution of Lin (1954); – –, finite strength blast solution of Bach & Lee (1969); — · —, a linear blast trajectory (i.e. constant blast velocity). The insert shows the same trajectories in linear coordinates.

3. The initiating blast wave and the cylindrical assumption

Experiments were first conducted in air in order to verify the hypersonic blast analogy assumption (see figure 1) and to establish its domain of validity. The blast trajectory from the 31, 94 and 537 kJ m^{-1} detonating cords were first measured. The bow shock trajectory was determined by the time of arrival of the shock front at fixed radial distances from the cord's axis. The detonation velocity V_{DC} of the high explosive in the cord determined experimentally is found to be $6.4 \pm 0.2\,\mathrm{km\,s^{-1}}$, independent of the cord size. The bow shock shape in the shock fixed (r, x) coordinates can be constructed from the (r, t) radial shock trajectory measured along a radius by using the simple transformation $x = V_{DC}t$ relating the axial coordinate to the time variable of the shock trajectory (see figure 1). The resulting bow shock shapes are shown in figure 3 for the different source energies. The radial and axial coordinates x and r in figure 3 are normalized by the characteristic explosion length R_0 (i.e. for a cylindrical blast, $R_0 \equiv (E_S/P_0)^{1/2}$). It can be seen that the three sets of data points collapse onto a same curve for shock radii greater than $\approx 0.1R_0$, as predicted by energy scaling from blast-wave theory. The fact that the results scale with the cylindrical explosion length suggests that the flow is quasi-cylindrical and reflects the cylindrical geometry once the blast is beyond a certain distance from the source. Similar results were obtained by Tsikulin (1960) for blast waves from long HMX detonating cords.

The approximation of a quasi-cylindrical flow field around a high-explosive detonating cord is in agreement with the hypersonic small-disturbance theory (Chernyi 1961). The theory is applicable to slender hypersonic projectiles, driving slender shocks. Mathematically, the conditions for validity of the hypersonic blast wave similitude are

$$M_x \gg 1, \tag{1}$$

$$\sin\theta_S \ll 1, \tag{2}$$

where M_∞ denotes the free-stream flow Mach number in a shock-fixed reference frame, and θ_S the local inclination angle of the shock wave. Under these conditions, the motion of the bow shock around a hypersonic body can be analysed conceptually in a laboratory reference frame as a series of infinitesimally thin cylindrical blast waves synchronized by the velocity of the hypersonic body, where the axial dependence can be neglected. The bow shock dynamics around the detonating cord clearly meet these conditions. In a shock fixed reference frame, the velocity of propagation in the axial direction is hypersonic:

$$M_{DC} \equiv \frac{V_{DC}}{c_0} \approx 18.4 \gg 1, \tag{3}$$

where V_{DC} is the detonation velocity in the cord and c_0 the sound velocity in the surrounding gas. The bow shock angle, as deduced from the measured shock (r, x)-trajectory, is indeed slender beyond the region in the immediate vicinity of the detonating cord axis. From our experimental shock trajectory of figure 3, for $R_S \geqslant 0.1R_0$, the shock angle, which is a decreasing function of shock radius R_S, satisfies the 'slender body' condition:

$$\theta_S \equiv \frac{\mathrm{d}R_S}{\mathrm{d}x} \leqslant 4^\circ \Rightarrow \sin\theta_S \leqslant 0.07 \ll 1. \tag{4}$$

Based on this quasi-cylindrical approximation, the radial shock trajectory, and consequently the shock shape, can be modelled by cylindrical blast-wave theory.

As a first approximation, the theoretical shock shape can be obtained from the classic similarity solution of Lin (1954) for a strong cylindrically expanding blast wave

$$R_S = \left(\frac{E_S}{\alpha_2\rho_0}\right)^{1/4} t^{1/2} = \left(\frac{E_S}{\alpha_2\rho_0}\right)^{1/4} \left(\frac{x}{V_{DC}}\right)^{1/2}, \tag{5}$$

where E_S is the energy per unit length of the source, and α_2 is a blast parameter, which is a weak function of the specific heat ratio γ (for air, $\gamma = 1.4$, $\alpha_2 = 0.986$). The corresponding shock strength can be obtained from the strong blast wave trajectory (5), by noting that the sound speed in the undisturbed gas can be written as $c_0^2 = \gamma P_0/\rho_0$, yielding

$$M_S = \tfrac{1}{2}(\alpha_2\gamma)^{-1/2} \left(\frac{R_S}{R_0}\right)^{-1}. \tag{6}$$

However, the strong blast solution is only accurate in the strong shock regime, i.e. for $M_S > 3$. For the moderate shock strength regime, the blast decay is approximated well by the perturbation solution of Bach & Lee (1969). In figure 3, the theoretical shock shape obtained from the perturbation solution and the similarity solution for cylindrical blast waves are compared to the experimentally determined shock shape. First, it can be seen that the shock trajectories obtained via the similarity solution for a strong shock and the perturbation solution for a finite-strength shock do not show any observable differences for shock radii less than $\approx 0.2R_0$, where the shock is strong. For shock radii greater than $\approx 0.1R_0$, excellent agreement is found between the experimental points and the perturbation blast-wave solution, whereas the similarity solution overestimates the rate of decay of the shock. This is not surprising, since the similarity solution is inaccurate for intermediate shock strengths (i.e. $M_S < 3$). The agreement between the theoretical perturbation solution and the experimental results confirms that the detonating cord yields the correct amount of energy per unit length.

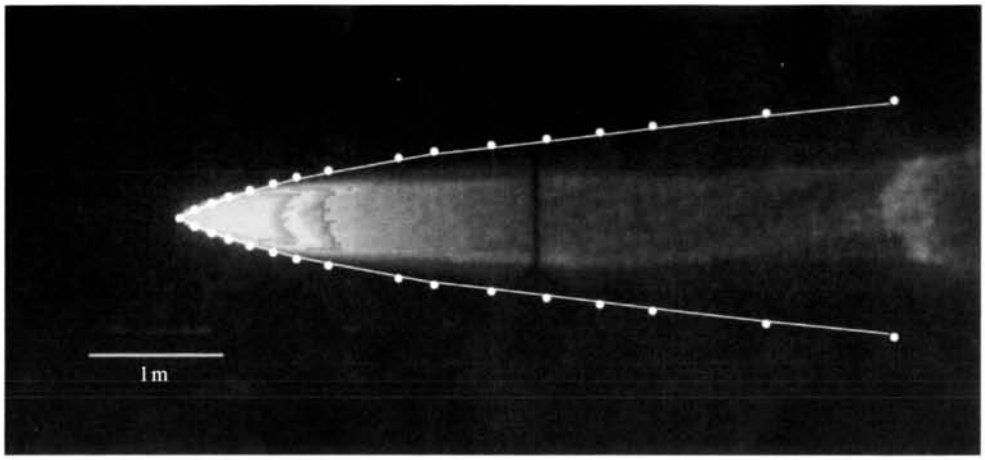

FIGURE 4. Self-emission photograph of the PETN products expansion in air from a $E_S = 537\,\mathrm{kJ\,m^{-1}}$ detonating cord; the bow shock wave was superimposed, as obtained from the trajectory measurements along one radius, using the relation $x = V_{DC}t$.

In the immediate vicinity of the cord, i.e. for shock radii less than $\approx 0.1R_0$, the blast trajectory deviates from the blast-wave solutions. In this region closer to the charge, the characteristic length scale governing the expansion of the detonating cord products influences the blast dynamics. Although the blast trajectory from the strongest cord ($537\,\mathrm{kJ\,m^{-1}}$) is closer to the ideal blast-wave solution than are the trajectories from the weaker cords, a general trend can be observed from the early blast trajectories. First, the decay rate of the blast waves measured appear to be significantly slower than predicted by strong blast-wave theory. More importantly, the early trajectories of the blast waves, for $R_S < 0.1R_0$, appear to be approximated well by a quasi-linear relationship $R_S \propto x$ (a power-law of slope 1 is indicated by a dot–dash line in figure 3). This implies that the shock angle ($\propto \mathrm{d}R_S/\mathrm{d}x$) and equivalently the velocity of the radial blast waves ($\propto \mathrm{d}R_S/\mathrm{d}t$) are nearly constant in this region. The nearly constant radial velocity of the blast wave in the near field is due to the piston effect of the expanding high-explosive products. This was confirmed by direct flow visualization of the expanding detonating cord products. A typical frame of the self-luminous high-explosive products from a $537\,\mathrm{kJ\,m^{-1}}$ detonating cord is shown in figure 4. The shock wave, although not directly visible in the photograph, has been superimposed, as obtained from the contact gauge measurements. Clearly, the early decay of the shock coincides to the radially expanding detonating cord products. Note that the maximum expansion of the PETN products corresponds to approximately the radius at which the blast decay first approaches cylindrical blast-wave theory, namely for $R_S > 0.1R_0 \approx 24\,\mathrm{cm}$ (cf. figure 3). At this radius, the chemical energy released in the high-explosive detonation, which initially went into raising the internal energy of the products, has been transferred into the surrounding gas as work done by the expanding detonation products. Once the PETN products stop expanding, the total useful energy has been deposited in the gas, and the subsequent gas motion can be described by ideal blast-wave theory. Similar effects of the asymptotic approach to ideal blast-wave theory have been observed for spherical blast waves resulting from finite radius high-explosive charges (Brode 1959).

The conclusion that can be reached from the above experiments in air is that the blast wave emanating from a long thin high-explosive detonating cord can be

modelled by cylindrical blast-wave theory for shock radii satisfying

$$R_S \geqslant 0.1 R_0. \tag{7}$$

In this region, both the non-ideal axial dependence and the influence of the expanding detonating cord products can be neglected. The quasi-cylindrical blast-wave can be analysed in the hypersonic blast wave analogy framework, by which the flow field is essentially decoupled in the axial direction. The finite detonation velocity in the cord synchronizes a successive series of cylindrical blast waves. This conclusion on the range of applicability of the hypersonic cylindrical blast-wave analogy is of prime importance for the subsequent study on direct initiation of detonation, when the detonating cord is surrounded by a combustible gas.

4. Direct initiation of detonation in combustible gas

4.1. *The supercritical regime*

As the blast wave generated by the detonating cord travels through a detonable gas, shock induced chemical reactions are triggered by the leading shock compression. If the blast wave is maintained sufficiently strong for a long enough time (i.e. high source energy equivalent to a slow decay rate of the blast wave), the chemical reactions remain coupled with the leading front of the blast wave and a detonation wave is initiated. This corresponds to the so-called supercritical regime of direct initiation. A typical sequence of side-on photographic records obtained for the supercritical regime is shown in figure 5. The detonating cord strength is $67\,\mathrm{kJ\,m^{-1}}$ and the ethylene–air equivalence ratio is 1.07. The successive frames are taken $143\,\mu\mathrm{s}$ apart, as the detonation in the cord moves towards the left-hand side in the pictures. The photographs are intentionally underexposed, to eliminate any background light and reveal only the strong self-emission of the gas combustion (blue in the photographs) and of the PETN products (orange–red in the photographs). It can be seen that the PETN products expand radially, forming an initially slender body of revolution that translates along the length of the cord at the detonation velocity in the PETN of the cord. Here, the analogy between initiation by detonating cord or by a hypervelocity projectile is clearly evident in these photographs. Also interesting to note is the successive re-compression and re-expansion of the detonating cord products, occurring at approximately 1.7 m behind the main detonation front in the cord. The second cone of intense luminosity is indicative of the secondary delayed shock wave driven by the re-expanding products. These subsequent slow pulsations of the high-explosive products and presence of secondary waves are analogous with the observations and analysis performed by Brode (1959) for spherical charges of high explosive.

Also visible on these high-speed photographs is the conical detonation wave in the surrounding combustible gas, which appears blue in the photographs. The half angle of this oblique conical detonation was estimated from the successive frames, yielding $\theta_S \approx 16.0 \pm 0.3°$. This is consistent with theoretical arguments for steady oblique CJ detonations, where the half cone angle θ_{CJ} can be simply evaluated from simple wave kinematics considerations (Higgins *et al.* 1998) in terms of the detonation velocity in the cord, V_{DC}, and the theoretical CJ detonation velocity, V_{CJ}, yielding

$$\theta_{CJ} = \sin^{-1}\left(\frac{V_{CJ}}{V_{DC}}\right) \approx \sin^{-1}\left(\frac{1.825\ [\mathrm{km\,s^{-1}}]}{6.4 \pm 0.2\ [\mathrm{km\,s^{-1}}]}\right) = 16.6° \pm 0.5°, \tag{8}$$

where the detonation velocity V_{CJ} was computed with the standard thermodynamic equilibrium code STANJAN (Reynolds 1986). The very good agreement between the theoretical and experimental shock angles, verified for different mixture compositions

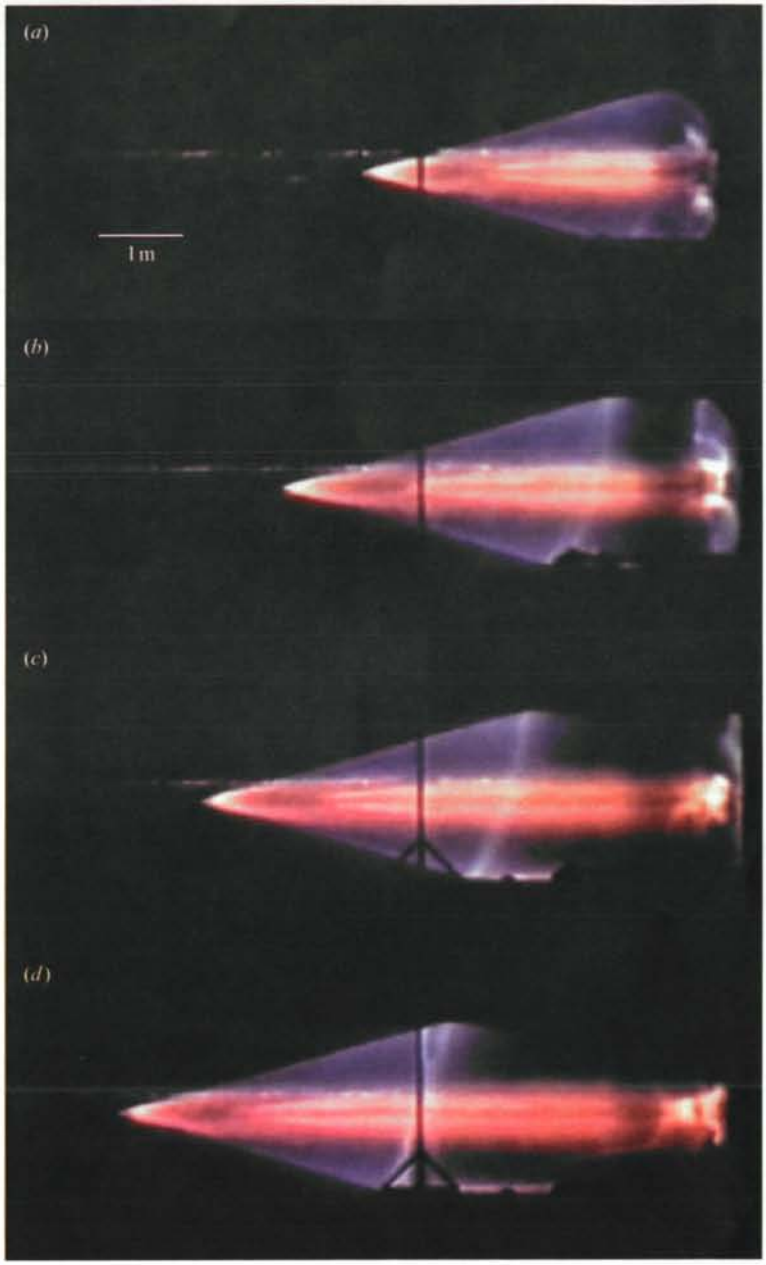

FIGURE 5. High-speed self-emission cinematography records illustrating the supercritical initiation of detonation in a C_2H_4–air mixture, $\phi = 1.07$, $E_S = 67\,\mathrm{kJ\,m^{-1}}$; the successive frames are taken at 143 μs intervals.

and cord strength in the supercritical regime, suggests that a stable CJ oblique detonation was initiated. The pressure measurements at the bag boundary are consistent with reflected pressure signatures behind multi-headed detonations. Analysis of the confining bag fragments after an experiment confirmed the multi-headed structure of the waves, with transverse wave spacings equal to those measured in unsupported CJ detonation (Murray & Lee 1984). Careful examination of the successive frames

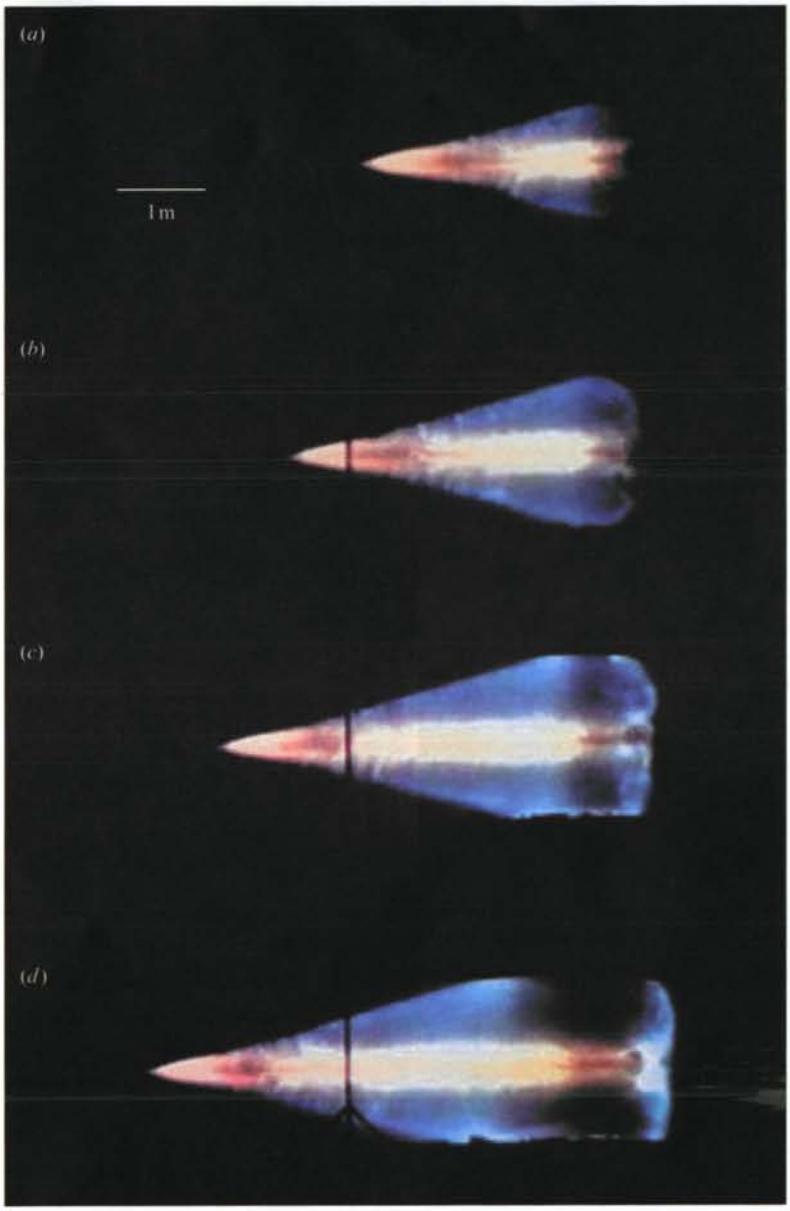

FIGURE 6. High-speed cinematography records illustrating the near-critical initiation of detonation in a C_2H_4–air mixture, $\phi = 1.03$, $E_S = 67\,\mathrm{kJ\,m^{-1}}$; the successive frames are taken at 143 μs intervals.

revealed that the flow field is steady and simply translating along the cord length. The existence and stability of CJ oblique detonations is thus confirmed (Pratt *et al.* 1991; Shepherd 1994).

4.2. *The critical regime*

As the critical conditions for initiation are approached (i.e. by decreasing the fuel equivalence ratio for a given strength of cord), the flow fields became increasingly more complex. Figure 6 shows four successive frames of an experiment conducted

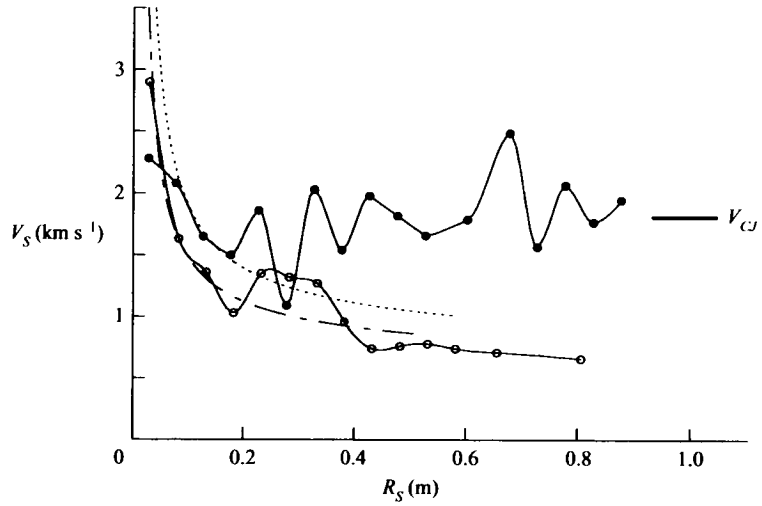

FIGURE 7. ●, Near-critical radial shock velocity profile and ○, subcritical velocity profile in C_2H_4–air, $\phi = 1.03$ for $E_S = 67\,\mathrm{kJ\,m^{-1}}$ and $E_S = 31\,\mathrm{kJ\,m^{-1}}$, respectively; the cylindrical reacting blast wave solution (11) for ···, $E_S = 67\,\mathrm{kJ\,m^{-1}}$ and – – –, $E_S = 31\,\mathrm{kJ\,m^{-1}}$.

in a slightly less sensitive mixture than above for the same strength of cord ($\phi = 1.03$, $E_S = 67\,\mathrm{kJ\,m^{-1}}$). The detonating cord initiated what appears as an oblique conical detonation. However, careful examination of the photographs indicates that the oblique detonation is concave, indicating an acceleration process as the wave propagates outward. The front appearing in the photographs is not smooth and consists of a series of periodic accelerations associated with intense three-dimensional chemical activity near the front. From the photographs, it can be seen that as the wave progresses radially, these irregularities disappear. Within the resolution of the photographs, the front becomes smooth and approaches a constant angle of approximately 16° before it reaches the bag boundary, suggesting that a CJ detonation was initiated. The local fluctuations in the acceleration process of the detonation front to CJ velocities are shown in figure 7, where the radial leading shock velocity was measured via 18 contact gauges mounted perpendicular to the cord. An overall acceleration process and oscillating behaviour are observed. Although the limited resolution did not permit a further quantification of these pulsating phenomena, this behaviour is typical of near-critical initiation conditions where the wave approaches a regular CJ detonation asymptotically (Edwards, Hooper & Morgan 1976).

When the mixture sensitivity was further reduced, phenomena of increased complexity were observed. A typical sequence of photographic records in this critical regime is shown in the successive frames of figure 8 for $E_S = 67\ \mathrm{kJ\ m^{-1}}$, $\phi = 1.00$. The blast wave no longer asymptotes to a conical CJ detonation wave. Instead, initiation is governed by the appearance of explosion centres, which originate at a radius of 22 cm away from the cord. Detonation 'bubbles' developed from these localized explosion centres. During the early phase of the bubble formation, only the transverse structure is indicative of bright luminosity, indicative of the high burning rate typical of detonative combustion. This was observed both from side-on photographs, as shown in figure 8, and from head-on photographs along the length of the detonation cord. Hence, detonative combustion is only observed initially in the longitudinal and azimuthal directions, and not in the radial direction where the combustion front propagates into the fresh mixture. Only at a radius of approximately

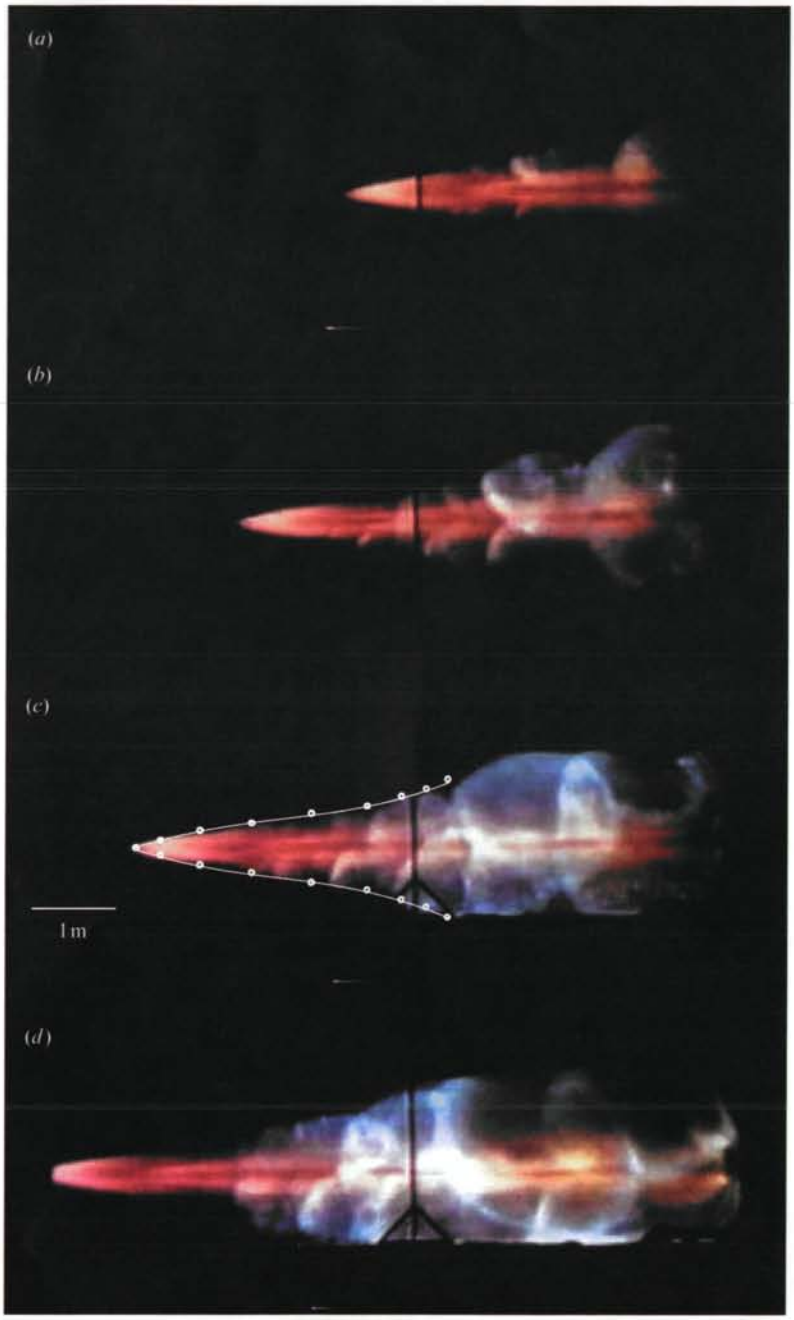

FIGURE 8. High-speed cinematography records illustrating the critical initiation of detonation in a C_2H_4–air mixture, $\phi = 1.0$, $E_S = 67\,\mathrm{kJ\,m^{-1}}$; the successive frames are taken at 200 μs intervals; the bow shock wave superimposed in (*c*) is obtained from the trajectory measurement along one radius, using the relation $x = V_{DC}t$.

60 cm from the cord's axis do the bubbles develop a bright normal front, suggesting the final onset of a CJ detonation propagating into the unburned gas. This behaviour was observed near the critical initiation conditions over the entire range of detonating cords investigated.

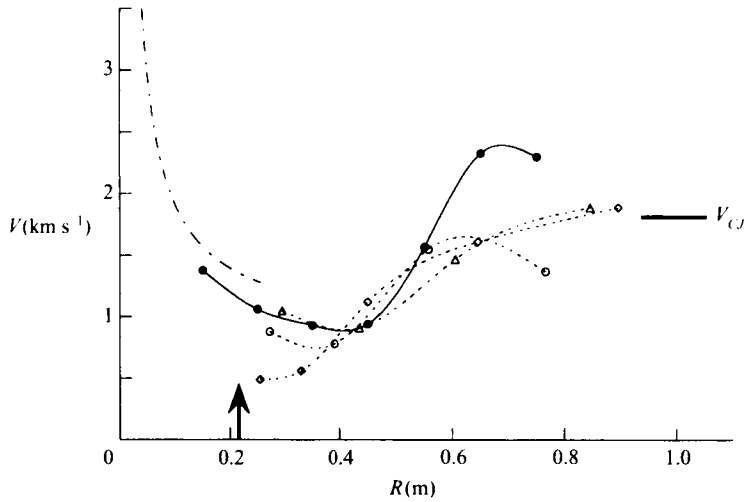

FIGURE 9. Radial velocity profiles for critical initiation in C_2H_4–air: ●, the shock velocity profile for (E_S = 67 kJ m^{-1}, ϕ = 1.0); ···, combustion front trajectories obtained from the three detonation kernels appearing in the successive frames of figure 10; – - –, the reacting blast wave solution (11); an arrow indicates the radius at which the onset of the detonation kernels in figure 8 and 10 is observed.

The continuous merging and amplification of detonation bubbles into CJ detonations along the length of the cord, although quite dissimilar locally, is globally reproduced in each successive frame of figure 8, suggesting a similar amplification time history for each detonation bubble. A record of the global acceleration of the leading shock along one radius is shown in figure 9, as measured from contact gauges. Cautious interpretation of this record is necessary, since the flow field is highly non-symmetric. In this sense, the velocity measurements only represent trends rather than quantitative information, especially towards the end of the record where detonation bubbles may overtake the recording 'sting' laterally. For a clearer interpretation of this velocity record, the corresponding shock trajectory has been superimposed arbitrarily on figure 8(*c*). The good agreement with the flow fields observed in the photograph suggests that it is representative of the acceleration process of the leading front until the final amplification of the detonation 'bubbles' at a radius of approximately 60 cm. The leading shock velocity record suggests that although the detonation centres appear on the photographs at a radius of 22 cm, the leading shock propagates steadily at approximately half the CJ value for some time, then accelerates to velocities greater than CJ at a radius of 60 cm. This is in excellent agreement with the photographic observations regarding the onset of bright luminosity in the radial fronts, suggesting that a self-sustained detonation propagating into the fresh mixture is only achieved at a radius of approximately 60 cm. The photographic observations also reveal some of the details of the intricate flowfield during this 'quasi-steady' period prior to onset of a regular detonation. After the first appearance of detonation centres, the leading front stops decaying while strong transverse fronts interact mutually in the transverse direction. The present experiments suggest that the amplification and establishment of a detonation wave is intimately linked with this system of interacting detonation kernels.

Near the limit of the critical regime, by further reducing the sensitivity of the mixture, a small number of explosion centres were sometimes observed to develop

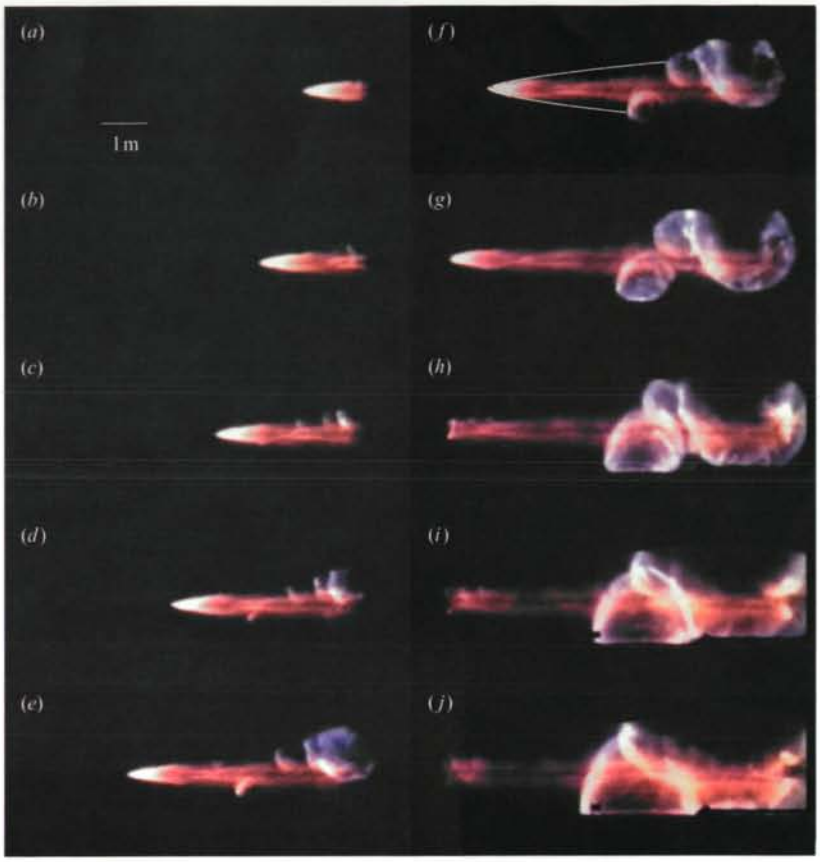

FIGURE 10. High-speed cinematography records illustrating the limit of the critical initiation regime of detonation in a C_2H_4–air mixture, $\phi = 0.98$, $E_S = 67\,\mathrm{kJ\,m^{-1}}$; the successive frames are taken at 143 μs intervals; the bow shock wave superimposed in (*f*) is obtained from the trajectory measurement along one radius, using the relation $x = V_{DC}t$.

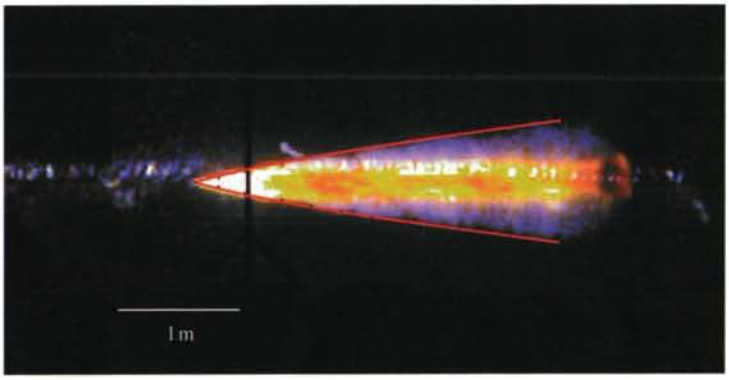

FIGURE 11. A high-speed digital video record illustrating the subcritical regime of detonation initiation in a C_2H_4–air mixture, $\phi = 1.03$, $E_S = 31\,\mathrm{kJ\,m^{-1}}$; the photograph was enhanced in the blue spectrum to reveal the less intense gaseous combustion; the bow shock wave superimposed was obtained from the trajectory measurement along one radius, using the relation $x = V_{DC}t$.

into local detonation bubbles, as can be seen in the successive frames of figure 10 ($E_S = 67\,\mathrm{kJ\,m^{-1}}$, $\phi = 0.98$). The density of these explosion centres was insufficient to merge into a conical detonation. Instead, as the detonation bubbles grew, a highly asymmetrical front was formed. In the regions affected by these explosion centres, the blast wave re-accelerated to the CJ velocity, while the rest of the blast wave decayed. Eventually, after the detonation in the cord exited the bag, the much slower gaseous detonation bubbles encountered the bag boundary and transitioned to a planar detonation covering the entire cross-section of the bag. The resulting detonation front propagated down the bag in pre-shocked gas at velocities close to the CJ velocity of the mixture.

The small number of explosion centres that appear on the records shown in figure 10 permitted an unambiguous analysis of the detonation bubble amplification into a self-sustained CJ detonation. The first conclusion is that these explosion centres consistently appear in a region very close to the cord. Within the resolution of the photographs' analysis, the explosion centres appear at a radius of approximately $22 \pm 2\,\mathrm{cm}$ away from the cord's axis, similar to the results reported above for slightly more sensitive mixtures. The end-on photographs confirmed the location of the onset of these detonation centres.

Although the shock wave is not seen in the successive frames of figure 10, it can be deduced from the luminosity details in the photographs. For instance, it can be seen that the morphology of the detonation centres displays a distinctive kink. This corresponds to the intersection of the decaying lead shock with the detonation kernel. For comparison, the approximate shock position is shown superimposed in figure 10(f), as measured from the contact gauges in a region unaffected by the detonation centres. Clearly, very good agreement is obtained between the distinctive kink in the left-hand side of the bubbles and the decaying shock. This triple point corresponds to the intersection between the decaying main shock, a strong transverse front propagating into shocked yet non-reacted gas, and the normal front of the detonation bubble. From the successive frames, it was determined that the intense-luminosity transverse fronts correspond to transverse detonation waves, propagating at velocities slightly less than CJ (~ 1.6–$1.7\,\mathrm{km\,s^{-1}}$) in the transverse direction into the shocked gas. This suggests that local detonative combustion has been initiated. However, the detonation centres do not propagate at CJ velocity in the normal direction, into unreacted gas. The velocity in the normal direction of each bubble, as deduced from the successive frames is shown in figure 9. Clearly, although the detonation centres are formed at approximately 22 cm away form the cord, CJ velocities are only reached at a radius of approximately 80–90 cm away from the cord, after a continuous acceleration. This long acceleration in the radial direction from initial velocities of $\approx 0.5 V_{CJ}$ confirms the earlier observations regarding the nature of amplification of the leading combustion front in the critical initiation regime. Presumably owing to the lower density of detonation bubbles, the acceleration process in the radial direction is somewhat longer. In some experiments at the limit of the critical regime, only one detonation bubble was observed, as the result of the interaction of the blast wave with the measuring sting. For these cases, although velocities near CJ were observed in the transverse direction, the normal part of the bubble did not accelerate to CJ velocity before reaching the bag boundaries. These observations also suggest the importance of multi-dimensional interactions in the amplification process of the combustion front to detonations.

In conclusion, it appears that the onset of detonation in the critical regime of initiation is governed by three-dimensional effects, where transverse detonation fronts

first appear, and propagate into shocked yet unreacted gas. The leading part of these detonating centres only slowly accelerates to a detonation on much longer length scales. The exact role played by the transverse detonations on the amplification of the normal front remains to be elucidated.

4.3. *The subcritical regime*

When the energy liberated by the cord is too weak and the shock decays too rapidly, the local detonation centres are quenched and detonation is not initiated. A typical photographic record corresponding to this 'subcritical' regime of initiation is shown in figure 11 ($E_S = 31\,\mathrm{kJ\,m^{-1}}$, $\phi = 1.03$). The high-speed digital video captured the gaseous reaction, which appears less intense than in a detonation. Intermittent regions of increased chemical activity are observed, indicating that the combustion zone is a turbulent deflagration. Owing to the decreased luminosity of these deflagrations, it was not possible to determine their velocity from the successive frames. Although the shock wave is not visible in the photograph in figure 11, the decay of the shock, as measured from contact gauges, is shown superimposed. The measured shock decay as a function of radius is also shown in figure 7. The leading shock wave decays first to approximately $0.6V_{CJ}$, followed by a short re-acceleration, and further decay. The short re-acceleration corresponds to the appearance of localized zones of chemical activity, as observed in the photographic record. However, they do not amplify to form detonation 'bubbles'. The leading shock, after propagating quasi-steadily at approximately $0.75V_{CJ}$ for 10 cm, completely decouples from the combustion region and decays to low velocities. In these subcritical initiation cases, the inability to form the strong transverse detonation fronts (detonation bubbles) does not permit the transition to detonation.

5. Discussion

A summary of the direct initiation experiments performed in this study is presented in figure 12. Each experiment is categorized as 'subcritical', 'critical' or 'supercritical', representing the cases of successful initiation of stable oblique detonations, unstable detonations, or failure to initiate detonations, respectively. As expected, for less sensitive mixtures (lower equivalence ratio), greater source energies per unit length are required. In the framework of oblique detonations and their stability, the degree of stability can be correlated with the proximity to the critical value of initiation energy. The present experiments reveal that the oblique detonations are stable except for a narrow 'critical' regime of initiation. In this sense, the stability of these oblique detonations does not depend on the dynamics of the self-sustained detonation, but rather on the details and repeatability of the initiation process itself. Since the detonation wave could never outrun the initiating source, which travels approximately at four times the gas detonation velocity, the apparent stabilization depends only on the ability of the generated blast wave to continuously directly initiate a detonation. In this sense, direct initiation theory provides the framework for analysing the stability of these oblique cylindrical detonations. For this reason, the subsequent discussion focuses on direct initiation theory and the unsteady flow fields resulting from the critical initiation regime.

Numerous phenomenological models relate the critical conditions for initiation to an experimental measure of the sensitivity of a detonable mixture (for review see, Benedick *et al.* 1986). The sensitivity of a mixture is reflected by the average spacing λ between the transverse waves forming the multi-headed structure of self-propagating

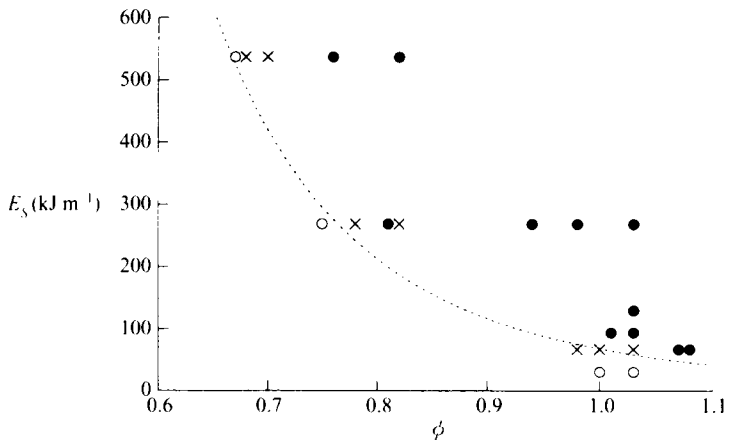

FIGURE 12. Summary of the detonation initiation experiments for different C_2H_4–air mixture compositions and strengths of detonating cord: ●, supercritical initiation; ×, critical initiation; ○, subcritical initiation; - - -, represents the $R_0^* \equiv \sqrt{E_S^*/P_0} \cong 30\lambda$ correlation.

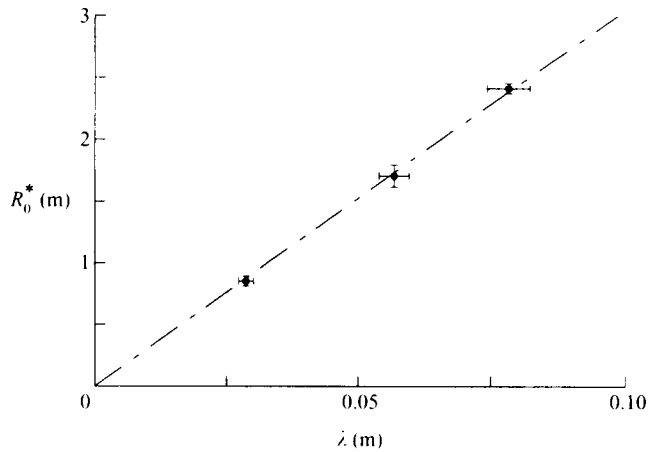

FIGURE 13. Critical cylindrical explosion length correlation with transverse wave spacing in C_2H_4 air mixture: - - -, $R_0^* \equiv \sqrt{E_S^*/P_0} \cong 30\lambda$.

detonations (Lee 1984). This length scale is representative of the spatial dimension of the unsteady hydrodynamic and chemical processes at the detonation front. On the other hand, a representative length scale for the self-similar blast decay is the explosion length R_0. For critical direct initiation, dimensional arguments suggest that the critical explosion length R_0^* be proportional to the cell size λ (Lee 1977).

The critical explosion radii determined in this study are shown in terms of transverse wave spacing λ in figure 13. The cell size measurements corresponding to each mixture composition were taken from the measurements of Knystautas *et al.* (1984), Murray and Lee (1984), and Moen *et al.* (1982, 1984), which were curve-fitted by a power law in the range of mixtures investigated. It yields

$$\lambda\,[\text{mm}] = 28.7\phi^{-2.55}, \tag{9}$$

for $0.6 < \phi < 1.2$. The cell size error bar in figure 13 represents the statistical uncertainty of (9) estimated from the scatter in the experimental measurements of approximately 5%. The critical explosion length uncertainty is estimated by using the one-to-one relationship between critical mixture composition and cord strength and the experimental scatter in critical mixture composition for a given strength of cord. The experimental results suggest a linear relationship between cell size and the critical explosion length for cylindrical blast initiation:

$$R_0^* \equiv \sqrt{\frac{E_S^*}{P_0}} \approx 30\lambda. \tag{10}$$

The fact that the critical conditions scale with the cylindrical explosion length confirms the earlier observations on the validity of the quasi-cylindrical assumption.

The numerical factor of proportionality in (10) may not be universal for all combustible mixtures, although similar approximates (i.e. $R_0^* \approx 20$–30λ) were reported for direct initiation of spherical detonations in different combustible mixtures (see, for example, Benedick *et al.* 1986; Desbordes 1986). Furthermore, it is important to note that the value of critical explosion lengths obtained here for the cylindrical geometry agree very well with the results obtained in the spherical geometry for the same combustible mixtures (Benedick *et al.* 1986; Radulescu *et al.* 2000), confirming the empirical observation that the critical explosion length is approximately invariant with geometry (Lee 1977). For a discussion on the invariance of explosion length, see Radulescu *et al.* 2000.

Although such an empirical correlation provides a practical means of estimating the source energy necessary for direct initiation of detonation, of more fundamental interest is the time history of the critical thermodynamic flow conditions occurring behind the initiating blast wave that is responsible for the onset of detonative combustion. Although our experimental technique does not provide a direct measurement of these parameters, they can be inferred by the knowledge of the blast front time-history itself. The blast trajectory in a reacting gas prior to the onset of detonation can be approximated very well by the self-similar blast motion where the contribution of the heat release from the chemical reactions is included in the blast motion analysis. Korobeinikov (1969) derives the early blast motion by treating the contribution from the chemical reactions as a second-order perturbation to the self-similar classic solution (6), yielding for the cylindrical case:

$$M_S = \tfrac{1}{2}(\alpha_2\gamma)^{-1/2}\left(\frac{R_S}{R_0}\right)^{-1}\exp\left(\frac{A_2 Q}{2M_S^2 c_0^2}\right), \tag{11}$$

where Q is the heat of reaction, α_2 and A_2 are dimensionless constants (Korobeinikov 1991 provides numerical estimates for the constants α_2 and A_2 for the different geometries and specific heat ratio), weak functions of the specific heat ratio γ. The theoretical blast decay (11) is shown superimposed to the experimentally measured shock trajectory for typical near-critical and subcritical tests in figure 7. The remarkably good agreement in the early phase of the initiation process, before the first velocity pulsation occurs, permits use of the theoretical trajectory as a very good approximation of the initiating blast-wave time history.

However, once the initiating blast wave has triggered detonative centres, the measured shock velocity profile does not provide an accurate measurement of the location where onset occurs, since the onset occurs from stochastically distributed explosion centres, which may not occur along the radius of measurement. The critical radius

at which the onset of detonation occurs can be determined from the photographic results, as the first appearance of detonation bubbles in the critical regime of initiation. Within the accuracy of our visualization results, we estimate the critical onset radius by

$$R_S^* \approx 0.26 R_0^* \tag{12}$$

with an accuracy of approximately 3%. First, we can see that the detonation onset length scale is well within the domain of validity, (7), of the cylindrical assumption (i.e. $R_S \geqslant 0.1 R_0$). This reconfirms the fact that the flow fields observed prior to the onset of detonation can be modelled satisfactorily by the cylindrical approximation. Furthermore, the present value of critical onset radius ($R_S^* \approx 7.8\lambda$) agrees well with the measurements reported by Higgins *et al.* (1998) and Vasili'ev & Grigoriev (1980) for direct initiation of cylindrical detonations in more sensitive mixtures.

The second parameter of great importance is the critical shock strength at which the onset of detonation occurs. Since the blast decay prior to the formation of the detonation centres is approximated very well by the perturbation solution for reacting blast waves, (11), this solution can be used to estimate the critical blast strength at the moment of explosion centre formation. Substituting (12) into the theoretical blast solution (11), and solving for M_S^*, we obtain

$$M_S^* \approx 0.75 M_{CJ}. \tag{13}$$

This value is in accord with the upper and lower bounds for critical Mach number deduced from the radial velocity profiles. For mixtures that are slightly critical, a minimum velocity 'dip' is observed at approximately $0.83 M_{CJ}$ (see figure 7) whereas for the critical regime, a quasi-steady complex is seen to propagate at approximately 0.5–$0.6 M_{CJ}$ after the initiation of detonation bubbles in the transverse direction (see figure 9).

The present experimental results for the critical energies and critical blast-wave parameters such as the shock strength and detonation kernel radius could be compared to recent theoretical models for direct initiation. In a recent study, Eckett *et al.* (2000) derive an analytical relationship for the critical energy for initiation based on a one-dimensional unsteady analysis of the chemical induction phase. They identify a critical decay rate of the blast wave that would lead to decoupling between the chemical reactions and the leading shock. However, the model has one free parameter and requires this critical decay rate to be evaluated at a critical shock strength M_S^*. We evaluated the model predictions of the critical energy for initiation for several values of M_S^*. At the experimentally determined value of $M_S^* \approx 0.75 M_{CJ}$, the model predictions exceed the experimental values for critical energies per unit length by approximately 2–5 orders of magnitude, depending on mixture composition. However, order of magnitude agreement can be obtained with $M_S^* \approx 0.86 M_{CJ}$. This order of magnitude change in predictions for very small changes in shock strength is due to the extreme sensitivity of induction time on local temperature and therefore on shock strength. To this effect, it is very difficult to assess the quantitative validity of the model before the critical shock strength is theoretically defined better in terms of dynamic and kinetic properties of detonations.

The cylindrical experiments may also be used simultaneously with experimental results obtained for other geometries (e.g. planar and spherical) to deduce some degree of universality regarding the critical conditions for direct initiation. To this effect, the experimental observation of invariance of the critical explosion length between the

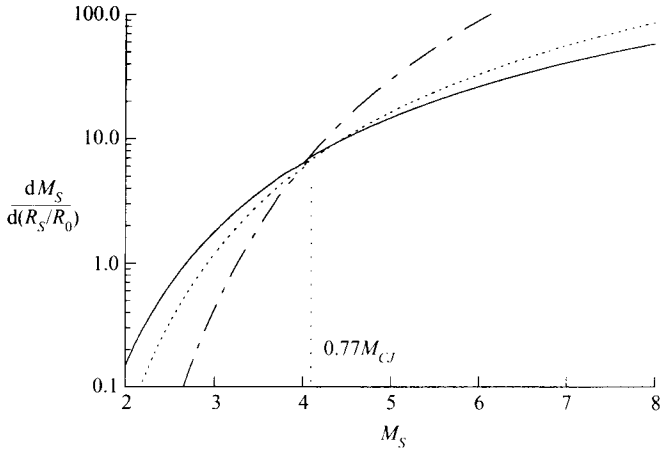

FIGURE 14. Normalized reacting blast wave decay rates, given by (14) as a function of blast strength for —, the spherical geometry; - - -, cylindrical geometry; – - –, planar geometry.

spherical, cylindrical and planar geometries (Lee 1977; Radulescu *et al.* 2000) provides a more stringent test for a theoretical model, since the model should reproduce the dependence between the critical energies for direct initiation in the three geometries. Since it was shown both numerically (Eckett *et al.* 2000) and experimentally in this study that the early blast decay is approximated very well by the Korobeinikov model (equation (11)), we can readily compare the theoretical decay rates from explosion length scaled blast waves in the different geometries. In figure 14, the decay rates for planar, cylindrical and spherical reacting blast waves given by Korobeinikov are plotted, normalized by the explosion length. The gas thermodynamic parameters used in the blast solution correspond to a stoichiometric ethylene–air mixture, although very similar profiles are obtained with different parameters. The non-dimensional decay rate, defined by

$$\tau_c \equiv \frac{c_0 t_c}{R_0} = \frac{\mathrm{d}(R_S/R_0)}{\mathrm{d}M_S}, \tag{14}$$

is approximately invariant at a blast strength of approximately $M_S \approx 4.1 \approx 0.77 M_{CJ}$. This shock strength corresponds to the critically observed shock strength in the present experiments. The conclusion that can be reached is that for an identical explosion length, blast waves for planar, cylindrical and spherical geometry exhibit similar decay rates at the critical blast strength observed experimentally. Since the invariance of explosion length was verified experimentally, this observation suggests that a critical decay rate criterion appears to be a correct criterion for direct initiation. Alternatively, in view of the present findings, models involving a critical wave curvature are inadequate to describe criticality in direct initiation (He & Clavin 1994).

Although a critical decay rate criterion for the initiating blast wave appears to be suitable for direct initiation, the assumption of strict one-dimensionality in previous direct initiation models is questionable, and may account for the large over-predictions for the critical initiation energies. In this sense, the intrinsic three-dimensional structure of detonations may be influential in permitting initiation in cases where a purely one-dimensional wave would fail. The three-dimensionality of the wave could also

account for the three-dimensional detonation kernels observed in the critical regime of initiation.

The flow fields observed by Edwards for direct initiation during the blast decay and its transition to a detonation revealed the importance of the three-dimensional cellular structure on direct initiation (Edwards *et al.* 1978). In their investigation of the critical flow fields near the energy source with the smoke foil technique, they observed that the frontal structure of the decaying blast waves is cellular, similar to that of self-propagating detonations. The transverse wave structure typically appears very early, where the blast wave propagates at velocities higher than CJ and the detonations are overdriven. As the blast decays, the spacing between transverse shocks increases. For large source energies, the rate of transverse wave disintegration during the initial decay is overcome by the rate of generation of new transverse waves within the reaction zone. In this case, the enlarged cells during the initiation phase multiply and evolve towards the self-propagating structure of detonations. Alternatively, for a rapid decay rate of the blast wave, the cellular structure completely disintegrates as the blast decays very fast. In the critical regime, the flow fields observed from the smoke foils indicated that owing to the irregularities in the detonation structure, some triple points may not completely disappear and can later give rise to discrete spots of detonation re-initiation. The spatial location of this decoupling and recoupling was observed during the first decay of the blast wave at approximately $0.65M_{CJ}$ in the mixtures investigated. The observations of Edwards serve to clarify the flow fields observed near criticality in the present experiments. The onset of detonation kernels observed in this study may be promoted by the vestigial transverse wave structure of the decaying reacting blast wave. This scenario may account for the fact that as the conditions for criticality are approached, the faster decay of the initiating blast wave dampens the potential re-initiation centres more and more effectively. Fewer surviving stochastic re-initiation heads remain active, which later amplify to form the detonation bubbles observed in the present experiments. If this picture is correct, it could be profitable to express the critical conditions for direct initiation by the balance between the rate of attenuation of the cell structure due to temperature drop and area divergence to the intrinsic rate of regeneration of new transverse waves from local instabilities in the reaction zone. Such a criterion, consistent with a critical decay rate of the initiating blast wave, would take into account the three-dimensional effects observed at the blast-wave front during its decay in combustible gas.

One further important conclusion from the present experiments is that whether a detonation is initiated or not in the far field is dictated by the appearance of the three-dimensional detonation centres during the initial blast-wave decay. Furthermore, contrary to the common belief of the quasi-instantaneous acceleration to CJ conditions upon appearance of detonation centres, the present experiments clearly illustrate the progressive amplification process. A 'quasi-steady' process is first observed at approximately half the theoretical CJ value, during which the detonative-like structures are observed only in the transverse direction. Since the leading shock is too weak for auto-ignition, only transverse detonative fronts initially amplify and ignite the pre-compressed gas. However, it is important to note that the further amplification of the detonations waves follow the events that are responsible for the onset of detonation, i.e. the onset of detonation kernels. Whether a detonation will be initiated or not is decided at this time, during the initial reacting blast wave decay. It can be concluded that a correct criterion for direct initiation should be applied at that time, irrespective of the flow fields generated after the onset of detonation kernels.

The authors wish to thank Teresa Mihalik, Keith Gerard and the entire technical staff at DRES for their valuable technical support in conducting the experiments. This research was supported by the National Sciences and Engineering Research Council of Canada (NSERC) and by the Defence Research Establishment Suffield (DRES) in Canada.

REFERENCES

AMINALLAH, M., BROSSARD, J. & VASIL'EV, A. 1993 Cylindrical detonations in methane–oxygen–nitrogen mixtures. *Prog. Astronaut. Aeronaut.* **153**, 203–228.

BACH, G. G. & LEE, J. H. 1969 Higher-order perturbation solutions for blast waves. *AIAA J.* **7**, 742–744.

BENEDICK, W. B., GUIRAO, C., KNYSTAUTAS, R. & LEE, J. H. 1986 Critical charge for direct initiation of detonation in gaseous fuel air mixtures. *Prog. Astronaut. Aeronaut.* **106**, 181–202.

BRODE, H. L. 1959 Blast wave from a spherical charge. *Phys. Fluids* **2**, 217–229.

CHERNYI, G. G. 1961 *Introduction to Hypersonic Flow*. Academic.

DESBORDES, D. 1986 Correlations between shock flame predetonation zone size and cell spacing in critically initiated spherical detonations. *Prog. Astronaut. Aeronaut.* **103**, 166–180.

DOBRATZ, B. M. & CRAWFORD, P. C. 1985 *LLNL Explosives Handbook*, UCRL-52997, Lawrence Livermore National Laboratory, CA.

ECKETT, C. A., QUIRK, J. J. & SHEPHERD, J. E. 2000 The role of unsteadiness in direct initiation of gaseous detonations. *J. Fluid. Mech.* **421**, 147–183.

EDWARDS, D. H., HOOPER, G. & MORGAN, J. M. 1976 An experimental investigation of the direct initiation of spherical detonations. *Acta Astronaut.* **3**, 117–130.

EDWARDS, D. H., HOOPER, G., MORGAN, J. M. & THOMAS, G. O. 1978 The quasi-steady regime in critically initiated detonation waves. *J. Phys.* D: *Appl. Phys.* **11**, 2103–2117.

HE, L. & CLAVIN, P. 1994 On the direct initiation of gaseous detonations by an energy source. *J. Fluid Mech.* **277**, 227–248.

HIGGINS, A. J., RADULESCU, M. I. & LEE, J. H. S. 1998 Initiation of cylindrical detonation by rapid energy deposition along a line. *Proc. Combust. Inst.* **27**, 2215–2223.

KNYSTAUTAS, R., GUIRAO, C., LEE, J. H. & SULMISTRAS, A. 1984 Measurement of cell size in hydrocarbon–air mixtures, and predictions of critical tube diameter, critical initiation energy, and detonability limits. *Prog. Astronaut. Aeronaut.* **94**, 23–37.

KOMATSU, M. & TAKAYAMA, K. 2000 Experiments of the transition from a deflagration driven shock wave to a detonation wave in three-dimensions. *Proc. 22nd Intl Symp. on Shock Waves.* (ed. G. Ball, R. Hillier & G. Roberts), vol. 1, pp. 321–326.

KOROBEINIKOV, V. P. 1969 The problem of point explosion in a detonating gas. *Astronaut. Acta* **14**, 411–419.

KOROBEINIKOV, V. P. 1991 *Problems of Point Blast Theory*. American Institute of Physics.

LEE, J. H. S. 1977 Initiation of gaseous detonation. *Annu. Rev. Phys. Chem.* **28**, 75–104.

LEE, J. H. 1984 Dynamic parameters of gaseous detonations. *Annu. Rev. Fluid. Mech.* **16**, 311–336.

LEE, J. H. S. 1997 Initiation of detonation by a hypervelocity projectile. *Prog. Astronaut. Aeronaut.* **173**, 293–310.

LEE, J. H. S. & HIGGINS, A. J. 1999 Comments on criteria for direct initiation of detonation. *Phil. Trans. R. Soc. Lond.* A **357**, 3503–3521.

LIN, S. C. 1954 Cylindrical shock waves produced by instantaneous energy release. *J. Appl. Phys.* **25**, 54–57.

MATSUI, H. & LEE, J. H. 1976 Influence of electrode geometry and spacing on the critical energy for direct initiation of spherical gaseous detonations. *Combust. Flame* **27**, 217–220.

MOEN, I. O., FUNK, J. W., WARD, S. A., RUDE, G. M. & THIBAULT, P. A. 1984 Detonation length scales for fuel–air explosives. *Prog. Astronaut. Aeronaut.* **94**, 55–79.

MOEN, I. O., MURRAY, S. B., BJERKETVEDT, D., RINNAN, A., KNYSTAUTAS, R. & LEE, J. H. 1982 Diffraction of detonation from tubes into a large fuel–air explosive cloud. *Proc. Combust. Inst.* **19**, 635–644.

MURRAY, S. B. & LEE, J. H. 1984 The influence of yielding confinement on large-scale ethylene–air detonations. *Prog. Astronaut. Aeronaut.* **94**, 80–103.

PRATT, D. T., HUMPHREY, J. W. & GLENN, D. E. 1991 Morphology of standing oblique detonation waves. *J. Propulsion* **7**, 837–845.

RADULESCU, M. I., HIGGINS, A. J., LEE, J. H. S. & MURRAY, S. B. 2000 On the explosion length invariance in direct initiation of detonation. *Proc. Combust. Inst.* **28**, 637–644.

REYNOLDS, W. C. 1986 The element potential method for chemical equilibrium analysis: implementation in the interactive program STANJAN. *Tech. Rep. Stanford University*, Department of Mechanical Engineering.

SHEPHERD, J. E. 1994 Detonation waves and propulsion. In *Combustion in High Speed Flows* (ed. J. D. Buckmaster, T. L. Jackson & A. Kumar), pp. 373–420. Kluwer.

TSIKULIN, M. A. 1960 Air shock waves from the explosion of a cylindrical charge of great length. *Prikl. Mekh. Tekh. Fiz.* **3**, 188–193 (in Russian).

VASIL'EV, A. A. 1983 Geometric limits of gas detonation propagation. *Fiz. Goreniya Vzryva* **18**(2), 245–249.

VASIL'EV, A. A. 1994 Initiation of gaseous detonation by high speed body. *Shock Waves* **3**, 321–326.

VASIL'EV, A. A. & GRIGORIEV, V. V. 1980 Critical conditions for gas detonation in sharply expanding channels. *Fiz. Goreniya Vzryva* **16**(5), 117–125 (in Russian).

ZELDOVICH, YA. B., KOGARKO, S. M. & SIMONOV, N. N. 1956 An experimental investigation of spherical detonation of gases. *Sov. Phys. Tech. Phys.* **1**, 1689–1731.